Composites Science and Technology 134 (2016) 217–225

Contents lists available at ScienceDirect

Composites Science and Technology

journal homepage: http://www.elsevier.com/locate/compscitech

Size effect of graphene nanoparticle modified epoxy matrix

Christian Leopold*, Wilfried V. Liebig, Hans Wittich, Bodo Fiedler

Technische Universität Hamburg-Harburg, Institute of Polymer Composites, Denickestrasse 15, D-21073, Hamburg, Germany

ARTICLE INFO

Article history:
Received 21 April 2016
Received in revised form
22 August 2016
Accepted 25 August 2016
Available online 27 August 2016

Keywords:
Nano particles
Stress concentrations
Fractography
Scanning electron microscopy (SEM)

ABSTRACT

The size effect of unmodified and graphene nanoparticle modified matrix fibres is experimentally investigated. Neat matrix fibres show a clear size effect of increasing tensile strength with decreasing volume due to a statistical defect distribution. The nanoparticle modified matrix shows no significant size effect. Nanoparticles act as crack initiators and consume fracture energy. The size of the particles is independent of specimen volume, so that the failure initiating as well as energy absorbing mechanisms are available, independently of the volume. Fractography analysis of SEM images shows different energy dissipation mechanisms such as micro-damage at the graphene particles. Graphene pull-out, layer separation, layer shearing, formation of micro voids as well as crack separation and crack bifurcation are observed that depend on the orientation of the graphite layers to the fracture plane. These mechanisms dissipate energy and so that a graphene nanoparticle modification result in an increased fracture toughness and thus increased strength of an epoxy matrix system if the volume is large enough. The maximum stress in specimen of small volume depends on graphene layer orientation, so that ideally, the covalent bonds of the nanoparticles should be orientated in loading direction.

1. Introduction

As fibre reinforced plastics (FRP) gain increasing importance as load carrying parts in many applications, accurate prediction of strength and failure behaviour becomes increasingly relevant. Size effects play an important role in the design and in the prediction of mechanical properties of composite laminates or parts. Size effects, meaning that the strength of a material decreases with increasing volume, are shown in literature to be present from a large to a smaller scale, regarding on laminate level the total volume or the thickness of the layers in a laminate [1–5], which gains increased importance since the development of thin-ply prepregs for producing composite laminates [6].

Regarding the substituents, size effects in fibres were first documented by Leonardo da Vinci for iron wires [7] and are shown to exist for different materials such as glass [8], carbon [9,10] or acrylic [11]. For polymer matrices, the microstructure and the stress state in the pure resin compared to the same material as a matrix in a composite may differ [12], which has to be regarded when comparing experimental data with FEM simulations and for estimation of the local strength of the matrix in the small volume between the fibres [13]. In an investigation by Hobbiebrunken et al. [14] a size effect for the RTM 6 epoxy matrix system was identified experimentally. By using dog-bone specimens and fibres of the same material, increasing tensile strength with decreasing volume was found [14].

Since the discovery of graphene in 2004 [15], it is used as a nanoparticle reinforcement for polymers and FRP with promising results for improving the mechanical properties amongst others. It was shown by Chandrasekaran et al. [16] in polymer nanocomposites that already the addition of small amounts of graphite nanoplatelets and graphene oxide increase the fracture toughness of the epoxy matrix by 25% respectively 40%. Rafiee et al. [17] reported “enhanced mechanical properties” such as Young's modulus, tensile strength and fracture toughness due to the addition of graphene nanoplatelets in epoxy nanocomposites at low nanofiller content. The graphene platelets performed better than carbon nanotubes. Also, higher resistance to fatigue crack growth with a graphene modification was shown [17,18].

The increase in fracture toughness and hence strength can be explained with stress relief due to micro-damage at the nanoparticles, such as graphene layer separation, layer shearing and formation of micro voids [16,19]. These mechanisms were already suggested for other layered particles as silicas by Wittich et al. [20]. In addition, crack pinning, crack deflection and crack branching at

* Corresponding author.
E-mail addresses: christian.leopold@tuhh.de (C. Leopold), wilfried.liebig@tuhh.de (W.V. Liebig), wittich@tuhh.de (H. Wittich), fiedler@tuhh.de (B. Fiedler).

http://dx.doi.org/10.1016/j.compscitech.2016.08.022

nanoparticles decrease the crack growth rate in polymer nanocomposites and thus increase the fracture toughness [16].

In graphene modified carbon fibre reinforced plastics (CFRP) these stress relieving mechanisms increase the fatigue lifetime [19]. Fractography analysis in CFRP laminates indicate different types of microdamage at graphene nanoparticles, but due to the complex crack geometry and large fracture surface, single damage mechanisms are hard to identify in composites [19]. Therefore, an approach for the investigation of very small volumes and thus smaller fracture surfaces by using fibres as specimens is presented.

In comparison to the question asked amongst others by Zweben in 1994 "Is there a size effect in composites?" [21] the question that arises now is that of a size effect in polymer nanocomposites and how microdamage at the particles influence the mechanical properties such as ultimate stress in a small volume. Small volumes are of particular interest for the use of graphene in FRP, because the matrix volume between the fibres in FRP is very small. The answer to this question as well as a better understanding of the different mechanisms of microdamage at graphene nanoparticles are the objectives of this work.

Usage of graphene in commercial products is rare [22], but due to their potential for improving mechanical properties of polymers or FRP, a better understanding of damage mechanisms may help finding possible applications for this promising material.

2. Experimental study

In this section the materials and the experimental program are described.

2.1. Materials and sample preparation

The resin Momentive Epikote RIMR 135 with the hardener Momentive Epikure RIMH 134 mixed in a ratio of 10:3 wt% are used as matrix system according manufacturer's recommendation. It is an epoxy matrix system with an amine hardener and has a glass transition temperature of $T_g = 93$ °C. Few layer graphene (FLG) Avangraphene-2 with less than six layers (according to the manufacturer) from Avanzare (Spain) is used as nanoparticle reinforcement for the modified fibres. The lateral size of the sheets is 5 μm–25 μm with thickness less than 2 nm (from the data sheet). According to the data sheet, the graphene particles are functionalised for their integration in polymers. The process for manufacturing neat and nanoparticle modified matrix fibres is shown schematically in Fig. 1. In a first step, only applicable for the modified fibres, the appropriate amounts of nanoparticles and epoxy resin are mixed inside a glove box before dispersion with a three roll mill (EXAKT Advanced Technologies GmbH 120E) that works on the principle of applying high shear rates on the mixture to disperse the nanoparticles homogeneously [23]. The mixture is fed into the three roll mill at the feed roll and collected at the apron roll. This process is repeated seven times with the gap widths being adjusted from 120 μm to 5 μm (Refer to Fig. 1). The rotational speed of the rolls is kept constant at 33 min^{-1}, 100 min^{-1} and 300 min^{-1} respectively. For the modified specimens, two configurations with 0.05 wt% and 0.1 wt% graphene nanoparticles in the matrix are produced. To the neat or the modified resin after the three roll mill dispersion the hardener is added and mixed manually for approximately 10 min and then degassed under vacuum for 15 min to remove any air inclusions.

The matrix fibre manufacturing process is adapted from Hobbiebrunken et al. [14]. In order to increase the viscosity for producing the fibres, the degassed matrix system is heated in an aluminium cup on a heating plate at a constant temperature of 50 °C for about 40 min. When the matrix starts to vitrify, the fibres are pulled with a needle. By dipping the needle into the matrix and lifting it, thin fibres stick to the needle. These fibres are wound around two rods (Refer to Fig. 1). The diameter can be adjusted to a certain point with the pulling speed of the needle. Fibres with diameters between 22 μm and 350 μm after curing are obtained. The fibres are cut and glued at one end on paper sheets, as shown schematically in Fig. 1. For avoiding tension stresses in the fibres because of thermal or chemical shrinkage during curing, only one end is fixed. Curing of the fibres is for 24 h at 20 °C and for 15 h at 80 °C as recommended for this matrix system. It is assumed, that any axial orientation of the molecule chains, which may have been occurred during stretching the resin into the fibre shape is lost during the curing process. Since the manufacturing process, including the curing cycle, is the same for all fibrous specimens and differences in the overall surface area of the fibres are small, the hardening reaction at atmospheric conditions is not considered for discussion of the test results. After curing the second end of the fibres is glued to the paper that is is prepared on the basis of the ASTM D3379 standard for single fibre tension tests [24] with a hole with dimensions of 10 mm × 25 mm.

In order to compare the obtained results with the strength of specimen with larger volume, dog-bone specimen are manufactured according to DIN EN ISO 527-2 [25] with a gauge length of $l = 30$ mm and a gauge width of $w = 3.86$ mm for the neat and $l = 13$ mm, $w = 4$ mm for the nanoparticle modified specimens respectively. The difference is due to manufacturing reasons.

2.2. Single fibre tension test and microscopy

The specimen, consisting of the fibres glued on the paper, is fixed in a universal testing machine (Zwick Z10) with a 10 N capacity load cell. Before testing the side bars of the paper, which connect the upper and lower part of the specimen are cut (Refer to Fig. 1). Tensile tests are executed with a test speed of 2 mm/min that is chosen in order to minimize plasticity effects with very high strains with necking and assure a more brittle failure mode of the fibres.

The cross section of the fibres after failure is lower than the original cross section because of necking during the test. Therefore, the cross section after failure is measured for each specimen in an optical microscope (Olympus BX51). The true failure stress R^t is calculated from the measured force at failure and the cross section area obtained by microscopy.

In order to determine the failure initiation and to study the failure mechanisms in detail, the fracture surface is observed by scanning electron microscopy (SEM) (Leo Gemini 1530). The SE2 detector with a working distance between 5 mm and 7 mm at 1 keV and without any sputtering of the surface is used.

The dog-bone specimens are tested with a universal testing machine (Zwick Z2.5) using a load cell with a capacity of 2.5 kN at a speed of 1 mm/min according to DIN EN ISO 527-2 [25]. As the testing speed may influence the strain at break and tensile strength, some dog-bone specimens of the neat configuration are tested with the cross-head speed of the fibre specimens of 25 mm/min for evaluation of this influence.

3. Results

In this chapter, test results of the tension tests are presented, showing the influence of specimen volume and nanoparticle modification on true failure stress. Representative stress-strain respectively load-displacement curves for dog-bone and fibre specimens are presented in Fig. 2. In case of the fibres, force displacement instead of stress-strain curves are given for better comparability among the specimens, because necking is visible

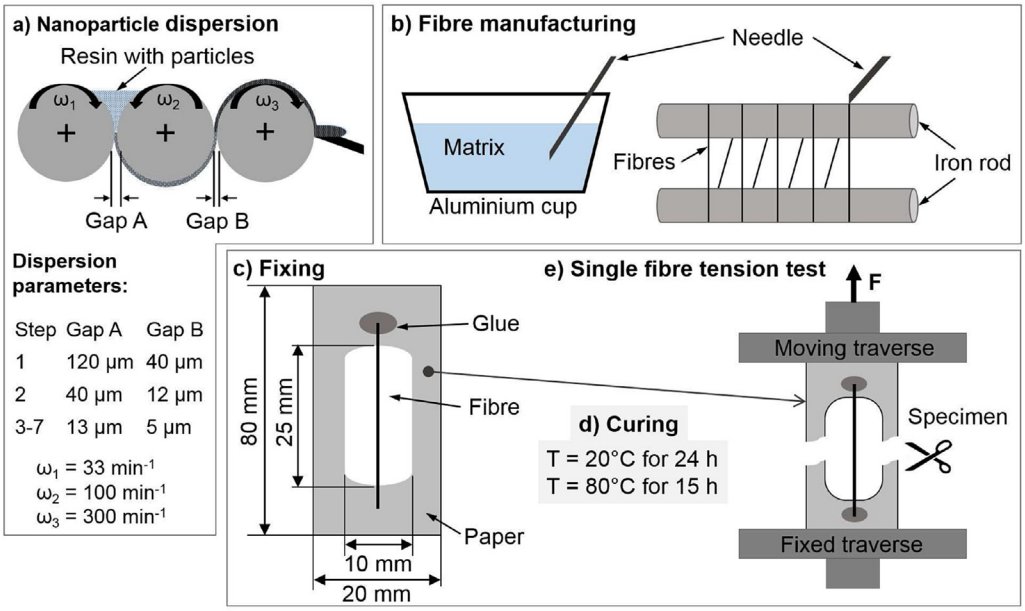

Fig. 1. Schematic representation of specimen manufacturing process: a) dispersion of nanoparticles in the resin (only for modified fibres) b) matrix fibre manufacturing c) specimen preparation for curing d) curing parameters e) scheme of test specimen mounted in universal test machine.

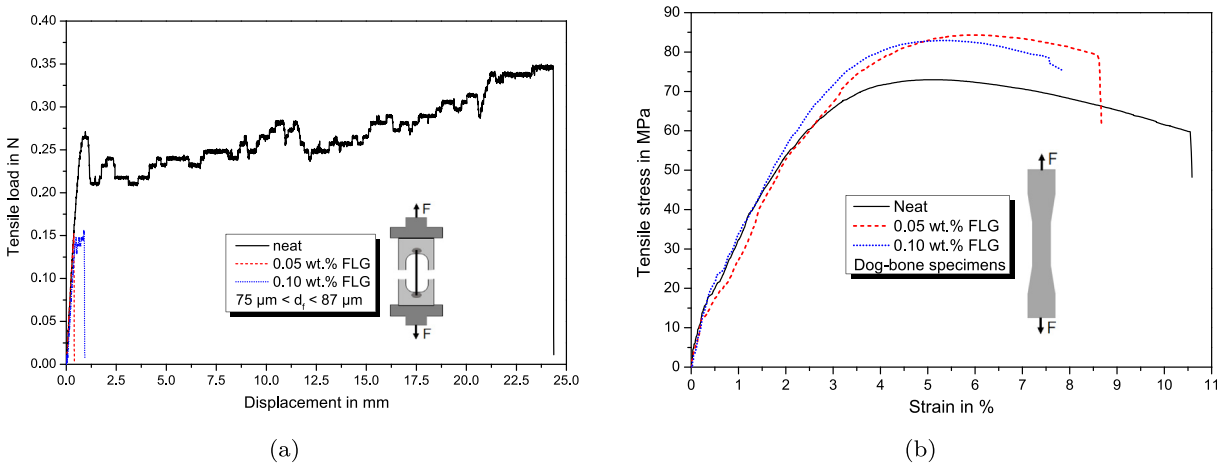

Fig. 2. Representative curves from tension tests: (a) Load-displacement curves for neat and FLG modified fibres of comparable diameter between 75 µm and 87 µm, (b) Stress-strain curves for neat and FLG modified dog-bone specimens.

during the test and has to be accounted for. The diagram for the fibres in Fig. 2(a) shows an increased elongation at break for the neat specimen in contrast to the comparable brittle failure of the nanoparticle modified fibres. For this diameter range, maximum load of the neat matrix is significantly (≈50%) higher. For larger fibre diameters however, maximum load can be in the same range for neat and modified fibres. For the dog-bone specimens (refer to Fig. 2(b)), a similar trend regarding the elongation is observed. The neat matrix exhibits higher ultimate strain. Nonetheless, maximum stress and failure stress are higher for the FLG modified specimens. With the force at failure and the cross section after failure, the true failure stress is calculated as described in Section 2.2.

Fig. 3 shows the true failure stress R^t for the neat fibres and dog-bone specimens as a function of specimen volume. The median value for failure stress of the dog-bone specimen is independent of their volume $R^t = 62$ MPa ± 3 MPa, which is in the typical range for the RIM 135 matrix system. According to the data sheet the strength is in the range of 60 MPa to 75 MPa. The neat specimen show a clear size effect. A decrease in volume leads to a significant increase in failure stress, with an improvement of up to 237% for the thinnest 22 µm fibre ($R^t = 209$ MPa) compared to the dog-bone specimen. The median value with standard deviation of true failure stress for the fibrous specimens is ($R^t = 121$ MPa ± 36 MPa), which is 95% higher than that of the dog-bone specimens. Even the lowest stress values for the fibres are approximately 20 MPa higher than those of the dog-bone specimens. The large scatter is attributed to the statistical defect distribution and the manual manufacturing process.

The true failure stress of the nanoparticle modified specimen in dependency of the volume is shown in Fig. 4. Results for fibrous and dog-bone specimen of the two configurations (0.05 wt% and 0.1 wt %) are presented. The degree of filling has no visible influence on the failure stress. Further investigations for a broader range of filling content may be necessary to verify this trend. The median

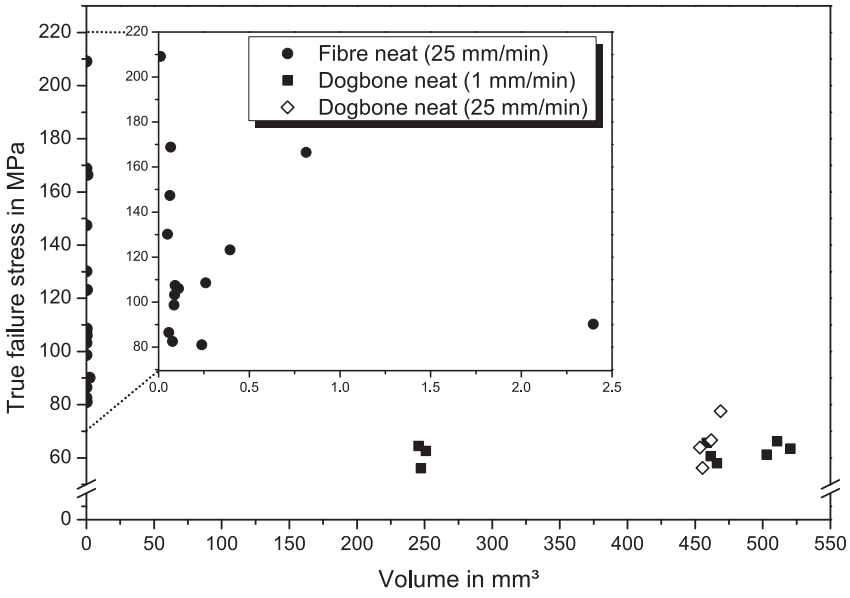

Fig. 3. True tensile stress R^t versus gauge volume V for neat epoxy matrix system.

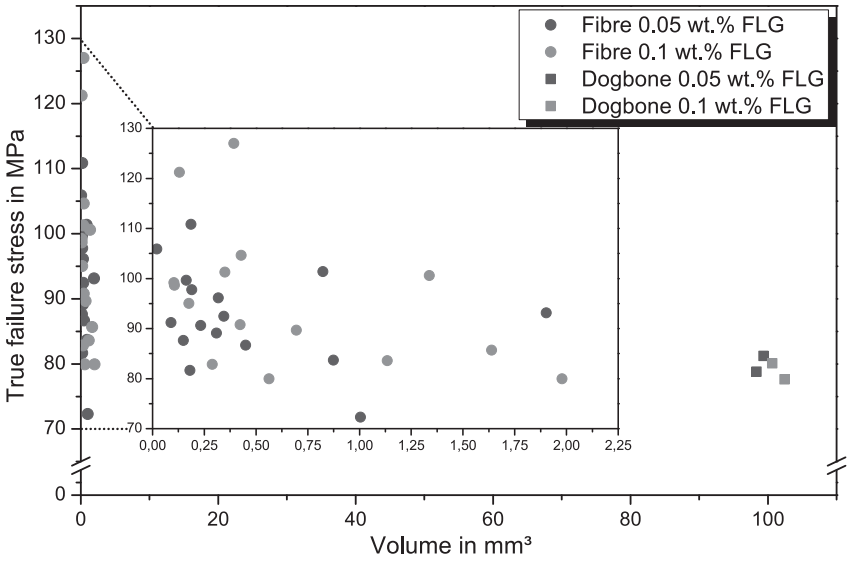

Fig. 4. True tensile stress R^t versus gauge volume V for graphene nanoparticle modified epoxy matrix system.

failure stress of the modified dog-bone specimen is ≈80 MPa, which is an increase of about 20 MPa (+29%) compared to the neat specimen. Since the true failure stress of the modified fibres with a median value of ($R^t = 93$ MPa ± 9 MPa) is only 16% higher compared to the dog-bone specimens, the modified matrix system shows only a small size effect, with a slight increase in stress with decreasing volume. When compared to the high increase for the neat matrix, the maximum failure stress for the modified matrix seems to be limited, even in very small volumes. These results implicate, that the nanoparticle modification act as an enhancement in larger volume, such as in the dog-bone specimens, but may weaken the material in very small volumes regarding the true failure stress. The reasons for this will be analysed using fractography and discussed in chapter 4. The cross-head speed seems to have no influence on the true failure stress. Values for all dog-bone specimens lay in the same range independent of the testing speed (refer to Fig. 3: dog-bone specimens tested at 25 mm/min are marked with open symbols). One specimen tested at 25 mm/min exhibits a slightly higher value, but this is more attributed to manufacturing quality than cross-head speed.

3.1. Fractography analysis

In order to investigate the reasons for final failure of the fibrous specimens, fractography of the fracture surfaces in SEM is carried out. Fig. 5 shows the fracture surfaces of three representative fibres of different diameter d and thus volume V, that failed at the stress given in the caption of the figure. The origin of failure, e.g. the flaw from which failure initiates, is marked in the pictures. Final failure initiates at surface defects in all neat matrix fibres, with the defect size being critical for ultimate failure stress. Since no rest lines are visible in the fracture surface, the crack growth rate is almost constant. The fibre in Fig. 5(a) has a very small volume and contains a very small surface defect and thus exhibits the highest failure

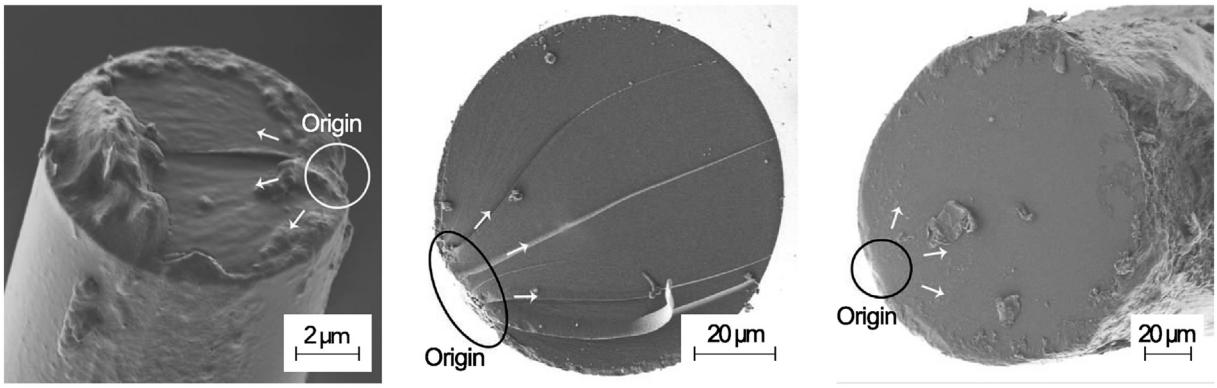

Fig. 5. SEM images of the fracture surface of neat matrix fibres of different volume V: (a) Neat fibre of volume $V = 0.01$ mm^3 ($d = 22$ µm) with true failure stress of 209 MPa (b) Neat fibre of volume $V = 0.24$ mm^3 ($d = 110$ µm) with true failure stress of 81 MPa (c) Neat fibre of volume $V = 0.81$ mm^3 ($d = 203$ µm) with true failure stress of 167 MPa.

stress, whereas for the fibre shown in Fig. 5(b) a larger defect results in a comparable low failure stress, which is even lower than that of the fibre shown in 5(c), although the later one has a larger volume. But as can be seen in Fig. 5(c), the surface area defect is smaller, than that of the fibre in Fig. 5(b) containing a surface defect nearly twice as large. This is attributed to the manufacturing process, during which the size of flaws varies statistically, so that also fibres of larger volume may as well contain a small defect. But in general, the trend of decreasing defect size with decreasing volume is observed. Therefore, these results are in good agreement with the theory of a statistical defect distribution [26].

SEM images of the fracture surfaces of three FLG modified fibres of different diameter are shown in Fig. 6, which failed at different strengths as given in the caption. Each fracture surface is representative for the respective range of true failure strength. The origin of failure initiation is marked in the images. Fig. 6(a) and (b) show fibres with 0.05 wt% and Fig. 6(c) a fibre with 0.1 wt% FLG dispersed in the matrix respectively. From the fractography analysis, the degrees of filling used in this study seem to have no influence on the fracture behaviour.

In contrast to the neat matrix fibres, where failure initiates from a surface defect, here the crack initiates from the largest FLG nanoparticle aggregate in the fracture surface in all modified specimens. As already mentioned, for the modified matrix the volume has minor influence on the strength, leaving particle size and orientation as reasons for the difference in strength. It is thus assumed that failure initiates at the largest particle or agglomerate in the volume, similar to the largest flaw in the neat matrix. But when comparing the two fibres shown in Fig. 6(b) and (c), the FLG particles at the origin of failure have nearly the same size. Despite having a smaller volume, the strength of the fibre in Fig. 6(b) is significantly lower, eliminating a size effect as explanation in this case. Regarding the fracture surfaces of the other fibres, this trend is confirmed. Hence, not only the size of the nanoparticle in relation to the fracture surface, but also its orientation with regard to the loading direction has an influence. Particle size alone is not the dominating factor for strength.

In Fig. 6d–f, larger magnifications of the failure initiating nanoparticle in the fracture surfaces shown in Fig. 6a–c respectively are shown. Different types of microdamage at the graphene nanoparticles are visible. Fig. 6(d) shows nanoparticle matrix debonding and a pull-out type of microdamage that occurs, when the graphene flakes are orientated in loading direction, because the interfacial strength between graphene and matrix is lower than the strength of the covalent atomic bonds within the graphene layers. Fig. 6(e) shows a flat, smooth and nanoparticle matrix debonding as well. The smooth surface indicates that two layers of graphene are separated from each other. This type of microdamage is typical for graphene layers being orientated perpendicular to the loading direction. In this case, the Van-der-Waals bonds between two layers fail before or at the same stress as the graphene matrix interface. In Fig. 6(f), shearing of two graphene layers orientated in an angle of approximately 45° to loading direction is visible. This is the case, when the Van-der-Waals bonds fail before the covalent bonds of the layers. Considering the tension test results and the fractography, the orientation of the largest particle has the highest influence on true failure strength. This is discussed further in chapter 4.

The fracture surface of all FLG modified fibres is rougher compared to the neat specimens. Crack deflection and crack bifurcation at other nanoparticles are clearly visible (refer to Fig. 6(b) and (c)). With this, the mechanisms for crack propagation in graphene nanoparticle modified epoxy matrix, proposed by Chandrasekaran et al. [16], are confirmed experimentally in a very small fracture surface.

4. Discussion

A clear size effect can be identified for the neat matrix, as expected from the theory of defect distribution that results in an increased strength with decreasing volume, as observed for the rupture of solids and brittle materials [8,26,27]. The strength for a brittle material under uniform stress is dominated by the largest defect. Defects are randomly distributed so that larger volumes have a higher probability of containing larger defects that results in lower strength. The size effect in solids with probability $P_i(\sigma)$ and critical stress σ_c as a function of the stress σ is described according to Weibull with equation (1) [26]:

$$P_i(\sigma) = 1 - \exp\left(- \left(\frac{\sigma}{\sigma_c}\right)^m \right) \tag{1}$$

where m is the Weibull-module. Fig. 7 shows the size effect in a Weibull weak-link-scaling (WLS) diagram for the matrix, in which the minimum values for true failure stress are plotted against volume on a log-log scale. The curve through these values to determine the Weibull-modulus m for the strength minima should be a straight line with a slope of $-1/m$. A Weibull modulus of $m = 0.28$ is calculated. In order to compare the tensile strengths $\sigma_{t,1}$ and $\sigma_{t,2}$ of

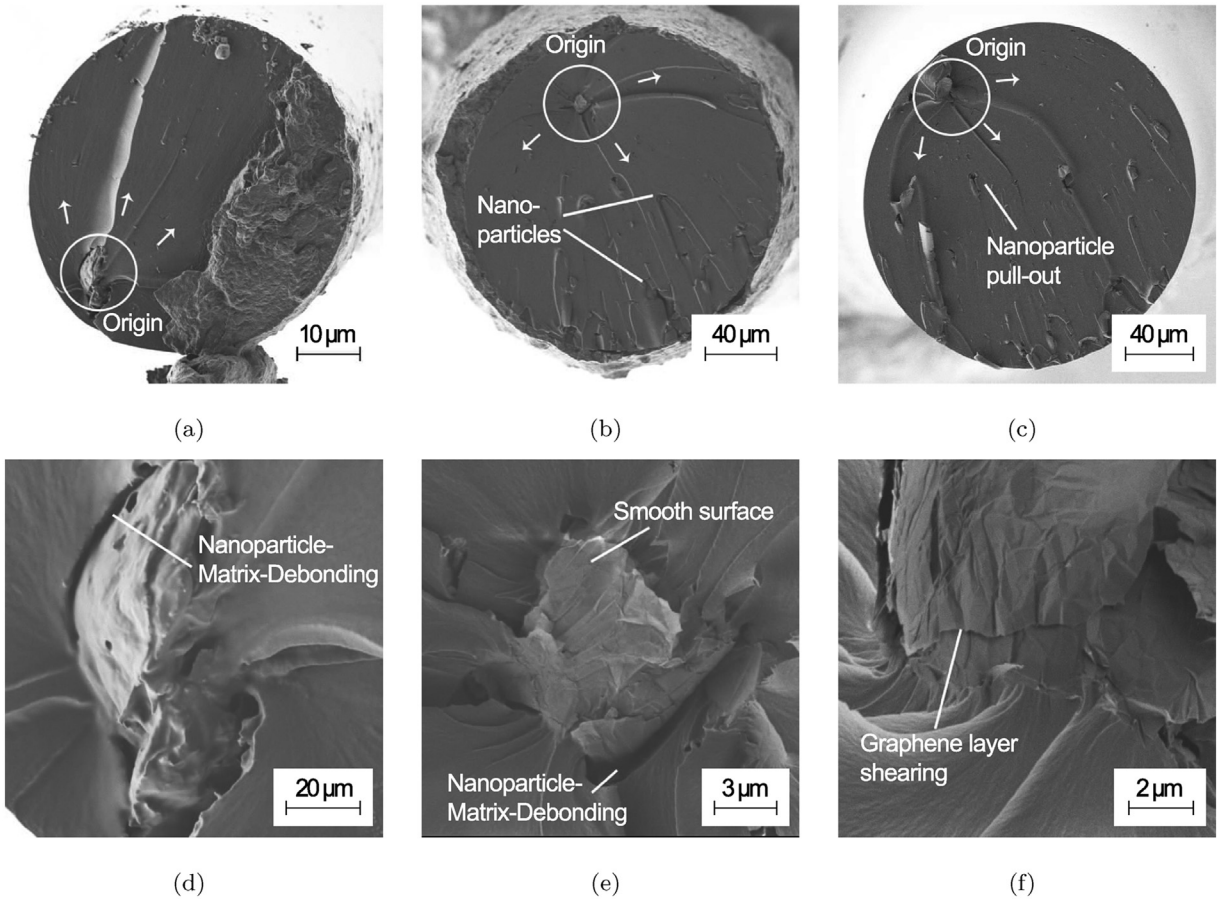

Fig. 6. SEM images of the fracture surface of neat matrix fibres of different volume V: (a) 0.05 wt% FLG modified matrix fibre of volume $V = 0.19$ mm^3 ($d = 97$ µm) with true failure stress of 111 MPa (b) 0.05 wt% FLG modified matrix fibre of volume $V = 1.00$ mm^3 ($d = 216$ µm) with true failure stress of 72 MPa (c) 0.1 wt% FLG modified matrix fibre of volume $V = 1.34$ mm^3 ($d = 261$ µm) with true failure stress of 101 MPa (d) Detail of (a), (e) Detail of (b), (f) Detail of (c).

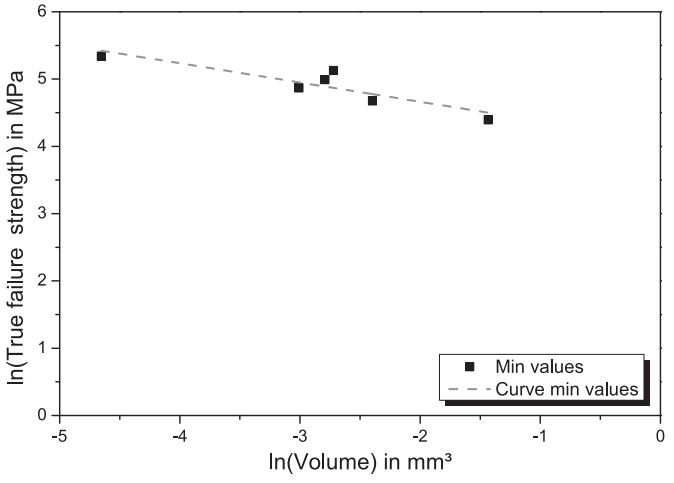

Fig. 7. Weibull weak link scaling diagram ($m = 0.28$).

two different volumes V_1 and V_2 equation (2) is used.

$$\frac{\sigma_{t,1}}{\sigma_{t,2}} = \left(\frac{V_1}{V_2}\right)^{-\frac{1}{m}} \tag{2}$$

Besides Weibull's theory, the Griffith criterion for the strength of a brittle material [8] can be applied as an analytical approach for estimating failure stress. According to this theory, the strength depends on flaws in the material. With the energy based criterion, the ultimate strength σ_{ult} of a material can be calculated with its stress intensity factor $K_{I,c}$ according to the following equation [8,28].

$$\sigma_{ult} = \frac{K_{I,c}}{\sqrt{\pi \cdot d_f}} \tag{3}$$

where d_f is the diameter of the fibre.

The maximum strength of a material is the theoretical strength, which is based on the separation of atomic bonds and thus the energy that is necessary to create a new fracture surface. It can be calculated with the following equation [29]:

$$\sigma_{th} = \sqrt{\frac{E \cdot G_0}{2h_p}} \tag{4}$$

where G_0 is the energy required to create a new fracture surface, h_p is the separation of the atomic planes and E is the Young's modulus of the material. For most solids the theoretical strength is $\sigma_{th} \approx E/10$ [29]. The measured strength values are lower than $E/10$ because of the presence of flaws. For plastic materials a theoretical strength of $E/30$ is derived, which is also postulated and applied as a lower bound for brittle ceramics [30,31].

In Fig. 8 the mentioned statistical (Weibull) or analytical

(Griffith) approaches to determine the strength of a brittle material in dependency of its volume are shown together with the obtained experimental results for the neat matrix. True tensile strength is plotted versus diameter in a ln-ln diagram. The theoretical strength, here assumed as $E/10$ [29], is shown in this diagram as well. For larger volumes, the experimental data is in good accordance with Weibull's theory of defect distribution, whereas for smaller volumes, as in the fibres, Griffith's failure criterion shows better agreement. For reaching the theoretical strength, the volume of the fibres is still too large. Flaws can be found in every fracture surface, so that the theoretical strength cannot be reached. Nonetheless, according to the authors knowledge, this is the first time, the strength to volume relation for polymers is described by different scaling laws and experimentally confirmed. It can be shown, that different scaling laws are valid for a polymer, depending on the range of specimen volume. Bauer et al. [31] presented this behaviour for ceramics on the nanoscale. Their investigations for nanoscale ceramics show, that when decreasing the volume further down, strength values are close or equal to the theoretical strength of the material [32] in compression or push to pull tension tests [31,32].

No significant size effect is visible for the nanoparticle modified fibres. As determined with fractography, failure initiates from a nanoparticle and not from a defect within the matrix material, therefore the statistical defect distribution has only minor influence on the true tensile strength in the fibrous specimens. The nanoparticles act as flaws in this context, counteracting any size effect due to differences in specimen volume, because there is always a nanoparticle and hence a crack initiating stress concentration present in the specimen. It is further assumed that failure initiates at the largest nanoparticle in the volume, similar to the largest flaw in brittle materials. From the lower strength of the modified fibres compared to the neat ones for small volumes it can be concluded that damage initiation at nanoparticles may lead to crack initiation in the small volume between the fibres in FRP at lower strength in static or at shorter time in cyclic tests.

When comparing the strength of the dog-bone specimens, the 29% increase in strength for the modified matrix is in accordance with previous investigations on the effect of graphene nanoparticles on mechanical properties of polymer matrices. A positive influence of FLG nanoparticle modification has been reported by several authors [16–19]. The increase in stress is attributed to a higher fracture toughness resulting from stress relieving mechanisms such as microdamage at the nanoparticles and crack separation and bifurcation [16]. In the nanoparticle modified fibres, the volume is too small for these stress relaxation mechanisms to be efficient, because any microdamage at a nanoparticle as first failure results in the final failure, leading to lower or equal strength compared with the neat fibres. Nonetheless are crack separation and bifurcation visible, confirming existing theories experimentally even in a small fracture surface. In the larger volume of the dog-bone specimens, microdamage does not result in final failure, but reduces the stress, which, along with a lower crack growth rate, leads to a higher stress compared to the neat material.

In the SEM images (refer to chapter 3.1), different types of microdamage at few layer graphene particles are observed that confirm existing models on damage initiation mechanisms at layered particles. In Fig. 9 a schematic representation of different types of microdamage at graphene nanoparticles with SEM images showing these types of damage in the fracture surface of FLG modified matrix fibres and the corresponding strength of the pictured fibres in a strength versus volume plot, are given. The schematic representation is based on the work of Wittich et al. for layered particles [20] and was already applied for explaining increase fatigue life of FLG modified FRP by Knoll et al. [19]. The type of microdamage depends on the orientation of the layers to the loading direction, as indicated in the scheme. Fibres in which the graphene layers of the largest nanoparticle in the fracture surface are orientated with the covalent bonds within the layers in loading direction exhibit the highest strength. When the graphene layers of the largest particle within the fracture surface are orientated perpendicular to loading direction, the Van der Waals bonds between the layers carry the load which results in lower strength (refer to the plot in 9 (c)) Thus, the true tensile strength is mostly determined by the orientation of the largest few-layer graphene nanoparticle with regard to loading direction. For best mechanical properties in a small polymer volume, in example the matrix between the fibres in FRP, the graphene layers should be orientated in loading direction. Further investigations are necessary to verify these results and to determine possibilities for controlled

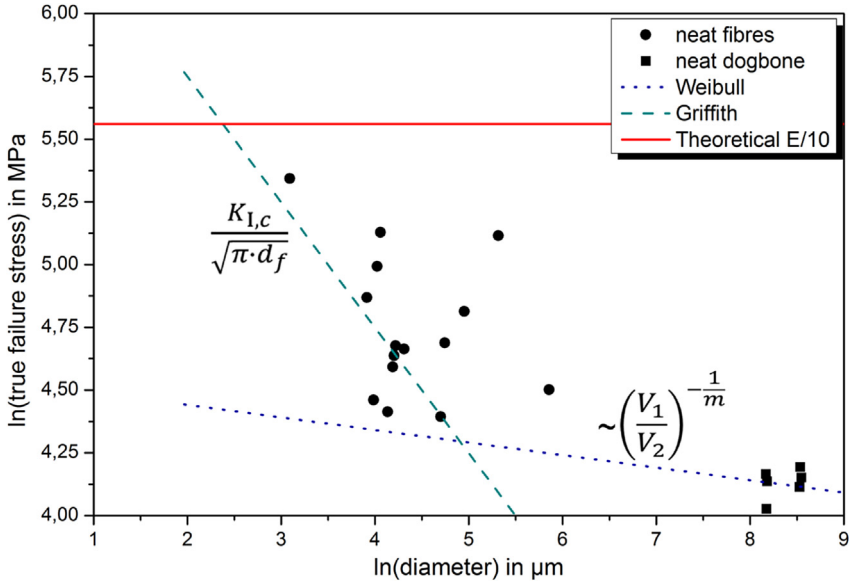

Fig. 8. Comparison of different analytical and statistical approaches for determining the size effect in polymers with experimental results.

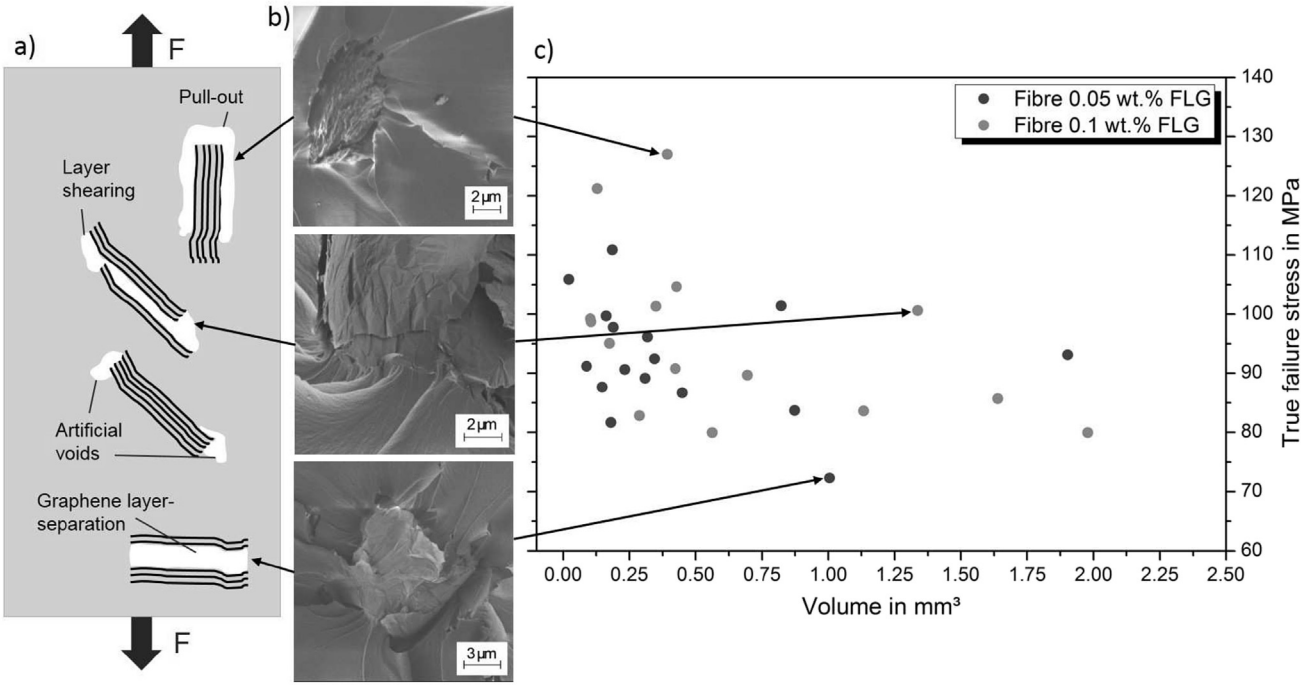

Fig. 9. Different damage mechanisms at FLG nanoparticles in dependency of the particle orientation with regard to the loading direction. a) Schematic representation of the mechanisms of microdamage after [19,20]. b) SEM images of the fracture surface of three different FLG modified matrix fibres showing the different mechanisms. c) True tensile strength versus specimen volume for the FLG modified fibres.

nanoparticle orientation in polymers.

5. Conclusion

The size effect of unmodified and graphene nanoparticle modified matrix fibres is experimentally investigated. A significant size effect that shows increasing tensile strength with decreasing volume due to a statistical defect distribution in neat matrix fibres is identified, which is according to Weibull's theory [26] and previous investigations for a different matrix system [14].

The nanoparticle modified matrix shows almost no size effect. Nanoparticles act as crack initiators and thus as flaws. The size of the particles is independent of specimen volume, so that the failure initiating as well as energy absorbing mechanisms are always available. In the fibres with their small volume and thus small crack area, this leads to failure initiation at the nanoparticles, counteracting any size effect due to a statistical defect distribution. In a bulk volume, energy dissipation mechanisms such as crack pinning, crack bifurcation and energy dissipation by micro-damage play a more important role, therefore higher values for tensile strength, compared to the neat matrix, are obtained with a nanoparticle modification as also reported in the literature [16,17,19,33].

Fractography analysis of SEM images shows different energy dissipation mechanisms. As micro-damage at the graphene particles are observed: Graphene pull-out, layer separation, layer shearing, formation of micro voids as well as crack separation and crack bifurcation. These mechanisms dissipate energy and so that a graphene nanoparticle modification result in an increased fracture toughness and thus increased strength [8] of an epoxy matrix system if the volume is large enough. With the identification of these single mechanisms, depending on the orientation of the graphene layers to the loading direction, theories and models about micro-damage at graphene nanoparticles are confirmed experimentally. The nanoparticle orientation with regard to loading direction influences the type of microdamage and thus the maximum stress in a specimen so that in a small volume ideally, the covalent bonds of the nanoparticles should be orientated in loading direction. Future investigations may clarify the influence of filling content for a broader range and may also focus on the influence of particle geometry, e.g. by using carbon nanotubes (longitudinal geometry) or carbon black (spherical geometry) as filler material.

Acknowledgement

The authors thank Benno von Essen for his help with manufacturing the fibres and executing the single fibre tension tests during his Bachelor thesis. This work was carried out with funding from the German Research Foundation (DFG) within the project number FI 688/5-1. This financial support is gratefully acknowledged.

References

[1] A. Parvizi, K.W. Garrett, J.E. Bailey, Constrained cracking in glass fibre-reinforced epoxy cross-ply laminates, J. Mater. Sci. 13 (1) (1978) 195–201.
[2] M.R. Wisnom, M.I. Jones, Size effects in interlaminar tensile and shear strength of unidirectional glass fibre/epoxy, J. Reinf. Plast. Compos. 15 (1) (1996) 2–15.
[3] J. Lee, C. Soutis, Thickness effect on the compressive strength of t800/924c carbon fibre–epoxy laminates, Compos. Part A Appl. Sci. Manuf. 36 (2) (2005) 213–227.
[4] J. Lee, C. Soutis, A study on the compressive strength of thick carbon fibre–epoxy laminates, Compos. Sci. Technol. 67 (10) (2007) 2015–2026.
[5] M.R. Wisnom, B. Khan, S.R. Hallett, Size effects in unnotched tensile strength of unidirectional and quasi-isotropic carbon/epoxy composites, Compos. Struct. 84 (1) (2008) 21–28.
[6] S. Sihn, R.Y. Kim, K. Kawabe, S.W. Tsai, Experimental studies of thin-ply laminated composites, Compos. Sci. Technol. 67 (6) (2007) 996–1008.
[7] R.W. Hertzberg, R.P. Vinci, J.L. Hertzberg, Deformation and Fracture Mechanics of Engineering Materials, fifth ed., Wiley, 2012.
[8] A. Griffith, The phenomena of rupture and flow in solids, Philos. Trans. R. Soc. Lond. Ser. A 221 (1920) 163–198.
[9] P. Rose, Hochfeste C-Fasern auf PAN-Basis, Einsatzformen und Eigenschaften im CFK-Verbund, in: Verarbeiten und Anwenden kohlenstoffaserverstärkter Kunststoffe, VDI-Verlag, Düsseldorf, 1981, pp. 5–39.
[10] D.J. Thorne, Carbon fibres with large breaking strain, Nature 248 (5451)

(1974) 754–756.
[11] D.J. Thorne, Distribution of internal flaws in acrylic fibers, J. Appl. Polym. Sci. 14 (1) (1970) 103–113.
[12] D. Hull, Matrix-dominated properties of polymer matrix composite materials, Mater. Sci. Eng. A 184 (2) (1994) 173–183.
[13] B. Fiedler, M. Hojo, S. Ochiai, K. Schulte, M. Ochi, Finite-element modeling of initial matrix failure in CFRP under static transverse tensile load, Compos. Sci. Technol. 61 (1) (2001) 95–105.
[14] T. Hobbiebrunken, B. Fiedler, M. Hojo, M. Tanaka, Experimental determination of the true epoxy resin strength using micro-scaled specimens, Compos. Part A 38 (2007) 814–818.
[15] K.S. Novoselov, A.K. Geim, S.V. Morozov, D. Jiang, Y. Zhang, S.V. Dubonos, I.V. Grigorieva, A.A. Firsov, Electric field effect in atomically thin carbon films, Science 306 (5696) (2004) 666–669.
[16] S. Chandrasekaran, N. Sato, F. Tölle, R. Mülhaupt, B. Fiedler, K. Schulte, Fracture toughness and failure mechanism of graphene based epoxy composites, Compos. Sci. Technol. 97 (2014) 90–99.
[17] M. Rafiee, J. Rafiee, Z. Wang, H. Song, Z. Yu, N. Koratkar, Enhanced mechanical properties of nanocomposites at low graphene content, ACS Nano 3 (12) (2009) 3884–3890.
[18] M. Rafiee, J. Rafiee, I. Srivastava, Z. Wang, H. Song, Z.-Z. Yu, N. Koratkar, Fracture and fatigue in graphene nanocomposites, Small 6 (2) (2010) 179–183.
[19] J. Knoll, B. Riecken, N. Kosmann, S. Chandrasekaran, K. Schulte, B. Fiedler, The effect of carbon nanoparticles on the fatigue performance of carbon fibre reinforced epoxy, Compos. Part A Appl. Sci. Manuf. 67 (2014) 233–240.
[20] H. Wittich, K. Hedicke, V. Altstädt, C. Mehler, Optimierung des Gefüges von Nanoplättchen aus Schichtsilikaten in Polymeren im Hinblick auf ihre mikromechanische Wirkung, in: Presented at 14. Symposium: Verbundwerkstoffe und Werkstoffverbunde, Austria, Vienna, 2003.
[21] C. Zweben, Is there a size effect in composites? Composites 25 (6) (1994) 451–454.
[22] E. Pullicino, C. Soutis, M. Gresil, Gambling with graphene…. will it pay off? JEC Compos. Mag. (99) (2015) 41–44.
[23] F. Gojny, M. Wichmann, U. Köpke, B. Fiedler, K. Schulte, Carbon nanotube-reinforced epoxy-composites: enhanced stiffness and fracture toughness at low nanotube content, Compos. Sci. Technol. 64 (15) (2004) 2363–2371.
[24] American Society for Testing and Materials, Standard Test Method for Tensile Strength and Young's Modulus for High-modulus Single-filament Materials, 1998. ASTM D3379.
[25] Deutsches Institut für Normung e.V., Plastics - Determination of Tensile Properties - Part 2: Test Conditions for Moulding and Extrusion Plastics, 1996, pp. 527–532. DIN EN ISO.
[26] W. Weibull, A statistical distribution function of wide applicability, J. Appl. Mech. 18 (1951) 293–329.
[27] W. Weibull, A statistical theory of the strength of materials, R. Swed. Inst. Eng. Res. 151 (1939) 1–45.
[28] D. Gross, T. Seelig, Fracture Mechanics, Springer, Berlin Heidelberg, 2011. Berlin, Heidelberg.
[29] A.J. Kinloch, R.J. Young, Fracture Behaviour of Polymers, Springer, Netherlands, Dordrecht, 1995.
[30] H. Gao, J. Baohua, I.L. Jäger, E. Arzt, P. Fratzl, Materials become insensitive to flaws at nanoscale: lessons from nature, Proc. Natl. Acad. Sci. U. S. A. 100 (10) (2003) 5597–5600.
[31] J. Bauer, A. Schroer, R. Schwaiger, I. Tesari, C. Lange, L. Valdevit, O. Kraft, Push-to-pull tensile testing of ultra-strong nanoscale ceramic–polymer composites made by additive manufacturing, Extreme Mech. Lett. 3 (2015) 105–112.
[32] J. Bauer, A. Schroer, R. Schwaiger, O. Kraft, Approaching theoretical strength in glassy carbon nanolattices, Nat. Mater. 2 (2016) 1–7.
[33] S. Chandrasekaran, W.V. Liebig, M. Mecklenberg, B. Fiedler, D. Smazna, R. Adelung, K. Schulte, Fracture, failure and compression behaviour of a 3D interconnected carbon aerogel (aerographite) epoxy composite, Compos. Sci. Technol. 122 (2016) 50–58.